Materials Innovations

HEXA Publishers

Textile Materials | Research Article | http://doi.org/10.54738/MI.2022.2101

Varied Morphological Study of Albite Nanomaterials at Low Temperature with Co-effect of Single Walled Nanotubes and Graphene Oxide for Kevlar Fabric Strength

Muhammad Arsalan Dilbraiz[1], Naveed Ahmed[2], Muhammad Tariq Javid[3], Amir Zada[4], Hameed Ullah Wazir[2], Saad Ahmed[5,6]*

1 Department of applied sciences, PNEC NUST, Karachi, 75350, Pakistan
2 Department of Chemistry, Hazara University, Mansehra, 21300, Pakistan
3 Department of Chemistry, Rawalpindi Women University, Setelite Town, Rawalpindi, 46300, Pakistan
4 Department of Chemistry, Abdul Wali Khan University, Mardan, 23200, Pakistan
5 Department of Chemistry, University of Okara, Okara, 56300, Pakistan
6 College of Chemical Engineering and Materials Science, Zhejiang University of Technology, Hangzhou, 310014, PR China

Received: 12 June 2021
Accepted: 25 January 2022
Published: 30 January 2022

Citation: Arsalan Dilbraiz M, Ahmed N, Javid MT, Zada A, Ullah Wazir H, Ahmed S (**2022**) Varied Morphological Study of Albite Nanomaterials at Low Temperature with Co-effect of Single Walled Nanotubes and Graphene Oxide for Kevlar Fabric Strength. *Materials Innovations 2* (1), 1-14.

***Correspondence**: (Saad Ahmed)
saadahmed@uo.edu.pk

Published By Hexa Publishers

ISSN
Electronic: 2790-1963

A comprehensive study of synthesizing zeolite nanoparticles, with the addition of organic template, by reflux method has been chalked out to form crystals. The method is effectivly for the synthesis of zeolite nanocrystals, incorporating alkali metals, silica and organic template. The organic templates tetra-propyl ammonium hydroxide (TPAOH), tetra-propyl ammonium bromide (TPABr) or (TPABr, N,N,N-tripropyl-1-propanaminiumbromide), tetraethyl orthosilicate (TEOS) were added to assist the formation of zeolite (Albite) crystals. A cross linker tetraethyl orthosilicate (TEOS) was also mixed. Addition of carbon nanotubes (CNTs) and graphene oxide (GO) resulted into a unique nano morphology of Albite (when the time of reaction was less than 240 h). Effect of additives on morphology, particle size, crystal geometry, surface area, and particle shapes was characterized with FT-IR, X-ray diffraction, BET, EDX and SEM. For the practical point of view, Kevlar supported polymer membrane with the Zeolite as catalyst is used. Results show that polymeric supported fabric and catalyst supported fabric have same result with response to mechanical testing. This suggest that the Kevlar supported polymer membrane has potential application in industrial cables, asbestos replacement brake lining, under water applications, tyres, and body armors.

Keywords: Synthesis, Albite, CNT, Surface Morphology, Porosity, Graphene oxide

INTRODUCTION

Zeolites are micro porous and hydrated aluminosilicate crystals composed of an infinity three-dimensional network of $[SiO_4]^{4-}$ and $[AlO_4]^{5-}$ tetrahedrally joined with each other through one oxygen atom at all possible sites to give a network, like a cage[1–2].

Owing to their high surface area, zeolites are predominately used in ion exchange resins, catalysis, adsorption, and molecular packaging. Pores in zeolite crystals at nanometer and sub nanometer level provide defining characteristics to zeolite to control shape selectivity on a molecular level[3−5]. Organic templates seem to be very important for the synthesis of desired and demanding pore size structure of zeolite crystal.

There is certain limitation of zeolites as well which are generally hindered the process for application. The limitation includes the micro porosity of bulky molecule, deactivation by irreversible adsorption, high acidic strength and the deposition of metal oxide to the active side of the substrate[6]. As the functional group have greater polarity it is very difficult to utilize the shape sensitivity of zeolites in chemical interactions. Whereas, the pore structure has an impact on selectivity and synthesis of cavity or pore sized material. This can affect the synthesis and application of the zeolites[7]. There are different methods used to synthesized zeolite nanoparticles. Hydrothermal method is the most common method used to synthesized nanoparticle of zeolite. The Si-O-Al is relatively easy to bond which will impart the crystallization around the particles under the induction of aluminum to formulate zeolite material[8−9]. Another method is phase transition that undergo solid-state transformation mostly undergoes decomposition reaction or changes in symmetry rather than overall structure. Sol-gel method is also used with reservations. High speed synthesis attracted the world by the Microwave method which relay on their speed due to significant enhancement in reaction rate, which depends upon pseudo-study state conditions. This implies with the sensitivity of the activated site of the substrate. Recently organic template assistant method is used to cater the problem. This method has advantages over other method due to its low cost, sensitivity, porosity, pore volume, nano synthesis and especially for environment friendly. I used organic template assistant method to control pore size, pore volume, surface area, crystallinity and also adsorption[10−11].

Zeolite are used to reduce cost for water purification and removing of heavy metals and ammonia. The physical properties of the zeolites are strongly affected by the presence and ratio of Si and Al. Secondly, the OH changes the nucleation time by inducing silicates to the solution phase[12−13]. Thirdly, the cation act as structure directing agent and balanced the framework. They also disturb the product concentration and purity level of crystals.The main problem is the cost and availability of the raw materials mainly the silica source for the synthesis of zeolite crystals. Silica, from sand having the different reactivity, selectivity and available in the form of the sol-gel and powder form. Silica and alumina chemicals as raw materials is more expensive[14−15]. So alternative material such as coal ashes, municipal solid wastes, clay minerals, incineration ashes and the industrial waste are the cheaper raw material for the Zeolite synthesis. The main purpose of synthesizing Zeolite is to reduce the environmental problems such as for the water purification and removing of the heavy metals and ammonia[16]. Zeolites act as catalysts for chemical reactions[17]. Essentially, Zeolites have essential properties, which make them particularly suitable as starting materials for the preparation of catalysts[18−19]. They are cation exchangers; hence it is possible to introduce a large variety of cations with different catalytic properties into their intra crystalline pore system, which in turn offers the opportunity to create different catalytic properties, e.g., in acid or metal-catalyzed reactions. Zeolites are crystalline porous materials with pore dimensions are in the same order as the dimensions of simple molecules hence they possess molecular sieving properties when the shape and size of a particular pore system exert a steric influence on the reaction, controlling the access of reactants and products[12,20−21].

Generally, Zeolite can be synthesized at high temperature that ranges from 600^0C to 900^0C from different time dilation. Template assisted highly depends upon the time dilation because at low temperature gel formation need some time to develop well define crystal of Zeolite and the assisted template can be removed at calcination temperature above 600 °C. Different research associate are believing that, with increase in temperature, variable nuclei can induce crystal formation[22−23]. However, crystallization process is slow process and we know that almost all natural occurring Zeolite often grow at low temperature with the base line of alkaline and saline lake system. The synthesis of Zeolite crystal must require a homogenized system of nuclei and simultaneously events leading to the formation of gel particle[24−25].

The recent research on template assisted Zeolite at moderate temperature have become a wide range of interest, in a desire pore size and geometry. Primarily we utilized tetra propyl ammonium hydroxide and tetra propyl ammonium bromide as in synthesis of zeolite Nano crystal. In that solution, alkaline cation amount should be appropriate to avoid flocculation of gel particles. The SDA groups needs very high temperature to establish porosity. One drawback is that these organic templates are mostly affected by environment and not very economical, so choice of the organic template is very important. Today, Zeolites are significantly used in variety of viable, military, and industrial applications, leading from water-softening in laundry detergents to chemical weapons. Kevlar is a synthetic fabric of para amide. Para phanyleneterephthalamide a very useful fabric and have important role in modern world in different fields.

It has a greater tendency to form a linear sheet like structure. It has a rigid molecules structure and favor a condensation reaction. It is a woven material which has high impact. It has low thermal conductivity. It has high tensile strength at low temperature as temperature increases with time its strength decreases. Due to its high tensile to weight ratio it is lighter as compared to steel. Therefore, it is used in many plastic fabric and many other materials. Kevlar fabric with the catalyst used to check fabric strength.

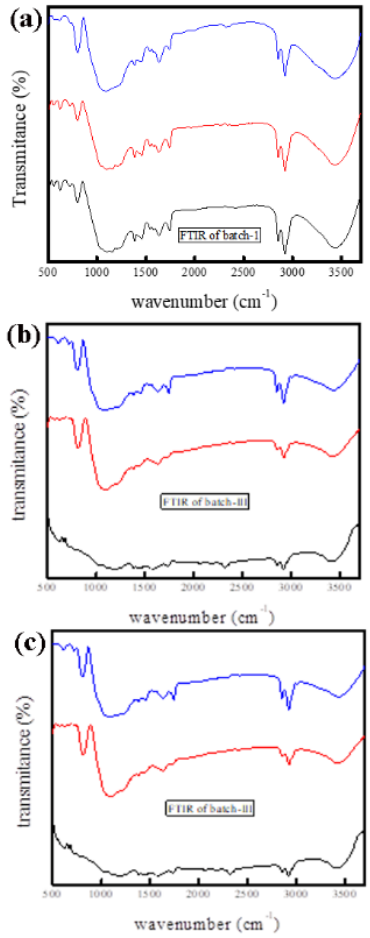

Figure 1. FT-IR Spectra (a) Batch-1 (b) Batch-II (c) Bach-III

Kevlar has three types and we used Kevlar 29 which is used in body armour, industrial cables, asbestos replacement, and brake lining and under water. Kevlar 29 is yellow in color, thickness ranges from 0.08 mm to 0.28 mm and its density is 1.44 g/cc. It is commonly known as Kevlar ballistic fabric. In support of this, we used polypropylene membrane with the addition of Zeolite to check its tensile strength.

EXPERIMENTAL SETUP

Materials and Methods

Sodium aluminum oxide ($NaAlO_2$), tetrapropyl ammonium hydroxide (TPAOH), tetrapropyl ammonium bromide (TPABr), tetraethyl orthosilicate (TEOS), nitric acid (HNO_3), sulphuric acid (H_2SO_4), hydrochloric acid (HCl) and graphene oxide (GO) were purchased from Sigma-Aldrich. Carbon nanotubes (CNT) were purchased from Sun Nanotechnology and functionalized it.

Batch-1: The samples of Batch-1 were prepared by taking the ingredients in two separate beakers labeled as A and B. 0.5 g of $NaAlO_2$ and 10 mL of TPAOH were added to beaker A and contents were stirred for 30 min followed by the addition of 10 mL deionized water. 10 g TPABr were mixed with 20 ml deionized water in beaker B and the contents were stirred at room temperature. Both the contents of beakers A and B were mixed TEOS was added drop wise and the mixture was refluxed for 240 h. During this time, samples were taken out after at an interval of 16 h, 32 h and 64 h.

Batch-2: The samples of Batch-2 were prepared by taking the ingredients in two separate beakers labeled as A and B. 0.5 g of $NaAlO_2$ was mixed with 10 ml TPAOH in beaker A and the contents were stirred for 30 min followed by the addition of 10 ml deionized water. 10 g TPABr were mixed with 20 mg of CNTs and the contents were stirred in 20 ml deionized water in beaker B at room temperature. Both the contents of beakers A and B were mixed TEOS was added drop wise and the mixture was refluxed for 240 h. During this time, samples were taken out after at an interval of 16 h, 32 h and 64 h.

Batch-3: The samples of Batch-3 were prepared by taking the ingredients in two separate beakers A and B. 0.5 g of $NaAlO_2$ was mixed with 10 mL TPAOH in beaker A and the contents were stirred for 30 min followed by the addition of 10 ml deionized water. 10 g TPABr were mixed with 100 mg of GO and the contents were stirred in 20 ml deionized water in beaker B at room temperature. Both the contents of beakers A and B were mixed and TEOS was added drop wise and the mixture was refluxed for 240 h. During this time, samples were taken out after at an interval of 16 h, 32 h and 64 h.

Application of synthesized zeolite

The thermal induced phase separation (TIPS) technique and dip coating method were used for this purpose. About 10 g isotactic polypropylene, 90 ml soya bean oil and 5 g adipic acid were heated in a beaker at 220 °C under constant stirring until the mixture became homogeneous. 1 g of the synthesized zeolite named as Albite or sodium TectoAluminotrisilicate was added under stirring till the mixture homogenized again. Then Kevlar fabric was dipped in the homogenized solution for about 10 sec and coated membrane was quench. The coated membrane was put into n-hexane for the removal of oil to form zeolite (sodium TectoAluminotrisilicate) composite polymer membrane and dried at 80 °C for 4 h.

Characterization

To study the crystal structure and its atomic spacing, X-ray diffractometry was recorded upon STOE Germany THETA-THETA diffractometer in 2 theta steps of diffraction. The anode material was made of Cu and the Scan Step Time was 0.4000 sec while Receiving Slit Size was 0.3000 mm at 25 °C. IR spectra in the

Table 1. Preparation of Na ($AlSi_3O_8$)

Sr. No	Reagents					pH	Product	Collection time (Hrs.)		
								S1	S2	S3
Batch – 1	$NaAlO_2$	TPAOH	TPABr	TEOS	——	10	Albite Na ($AlSi_3O_8$)	16	32	64
Batch – 2	$NaAlO_2$	TPAOH	TPABr	TEOS	CNTs	10	Albite Na ($AlSi_3O_8$)	16	32	64
Batch – 3	$NaAlO_2$	TPAOH	TPABr	TEOS	GO	10	Albite Na ($AlSi_3O_8$)	16	32	64

range of 4000-400 cm^{-1} were measured by using FTIR spectrometer of PerkinElmer Company (Spectrum 100 series). Brunauer-Emmett-Teller (BET) were performed on Micromeritics instrument corporation model Gemini VII 2390 (V1.03). Scattering electron microscopic images were recorded on JEOL JSM-6490A. Electron diffraction spectroscopy were performed on JEOL model JED-2300 analysis station.

RESULTS & DISCUSSION

FT-IR study of the samples

The FTIR spectra of the fabricated samples are given in Figure 1. The IR peaks in the range between 1100 to 900 cm^{-1} show stretching vibration of silicate in the samples [26]. The Si-O stretching and O-H bending bands are found in the range of 1300 to 400 cm^{-1}[27]. The peak below 900 cm^{-1} shows Al-O and Si-C band stretching. The peaks at 726 cm^{-1} and 670 cm^{-1} are for the symmetric stretching vibrations of Si-O-Si and Si-O-Al bridged bonds respectively. Obviously, high intensity of the symmetric stretching vibrations of Si-O-Si indicates the progress of the silicon condensation process [28–29]. The -OH stretching vibration between 3800-3200 cm^{-1} regions is due to adsorbed water molecules. In the IR spectrum of Batch-2 and Batch-3, the peaks at 3800-3200, 2950, 1400, 1800-1500, 1100-900 and 800 cm^{-1}, are assigned respectively to the O-H, Si-O, C-C, C=C, C-H, Al-O, Si-C and mineral hydrated silicate[30–36].

SEM study of the samples

Figure 2 shows the SEM images of the Batch-1 samples. It is obvious that particles size ranges between 20-100 nm for Zeolite (Albite) collected after 16 h as shown in Figure 2 (a) and (b). Images shows a gap between the particles. The images in Figure 2 (c) and (d) represent samples collected after 32 h. Obviously, particles are in regular shape but bigger in size compare to those collected after 16 h. The SEM images of the samples collected after 64 h are in the range of 20-100 nm and show big junks of zeolite (Albite) comprised of small particles.

Figure 4 (a) and (b) show the SEM images of Batch-2 samples obtained after 16 h of processing. In this case, the particles size range between 20-50 nm having regular geometry of CNTs doped zeolite. Figure 4 (c) and (d) show the SEM images of zeolite-CNT sample received after 32 h. The particle siz e is in the range of 50-100 nm and possess big junks formed from small particle. As the size increases, pore size decreases.Figure 4 (e) and (f) show SEM images of the Batch-2 samples collected after 64 h and most of the particles are rod like in the range of 50 nm. The size of the crystal goes on increasing it ranges up to 100 nm.

Figure 6 represent SEM images of the Batch-3 samples. The Figure 6 (a) and (b) show SEM images of the samples obtained after 16 h. obviously, particles are granular in shape with regular geometry and sizes of the crystal are between 40-50 nm. The granular shape of the crystal of zeolite is modified with the addition of graphene oxide as additive. As time is increased, the size of the crystal increase as shown in the Figure 6 (c) and (d) for the samples collected after 32 h. When time is further increased up to 64 h, the particles further grow in size and reached to 100 nm or even bigger up to 200 nm.

EDX Spectroscopic study of the samples

The presence of different elements in the fabricated samples of all the three Batches were determined using energy-dispersive X-ray (EDX) spectroscopic technique. The EDX spectrum of Batch-1, Batch-2, and Batch-3 samples is provided in Figure 3, 5, and 7, respectively.. It is clear that the fabricated Zeolite has the elemental composition of sodium, aluminum, oxygen, and majorly silicon. The other unidentified peaks may be related to the line peaks of sample holder.

The EDX spectrum in Figure 5 shows that the Batch-2 samples are mainly composed of aluminum, oxygen and silicon while those of Batch-3 samples contained silicon, oxygen, aluminum and sodium as shown in Figure 7. The unidentified peaks in all the three Batches may be related to the line peaks of sample holder.

X-ray Diffraction (XRD Analysis)

In Figure-8, matches the XRD pattern of Sodium TectoAluminotrisilicate (PDF reference no.01-072-1245). From the pattern it is clear that the sample has composition of Na, Al, Si, and O and confirmed sodium aluminum silicate (Zeolite family) in Anorthic crystals. Mineral name of this pattern is Albite. Sodium TectoAluminotrisilicate formulated as Na ($AlSi_3O_8$). The unit cell of the crystal has a spec-

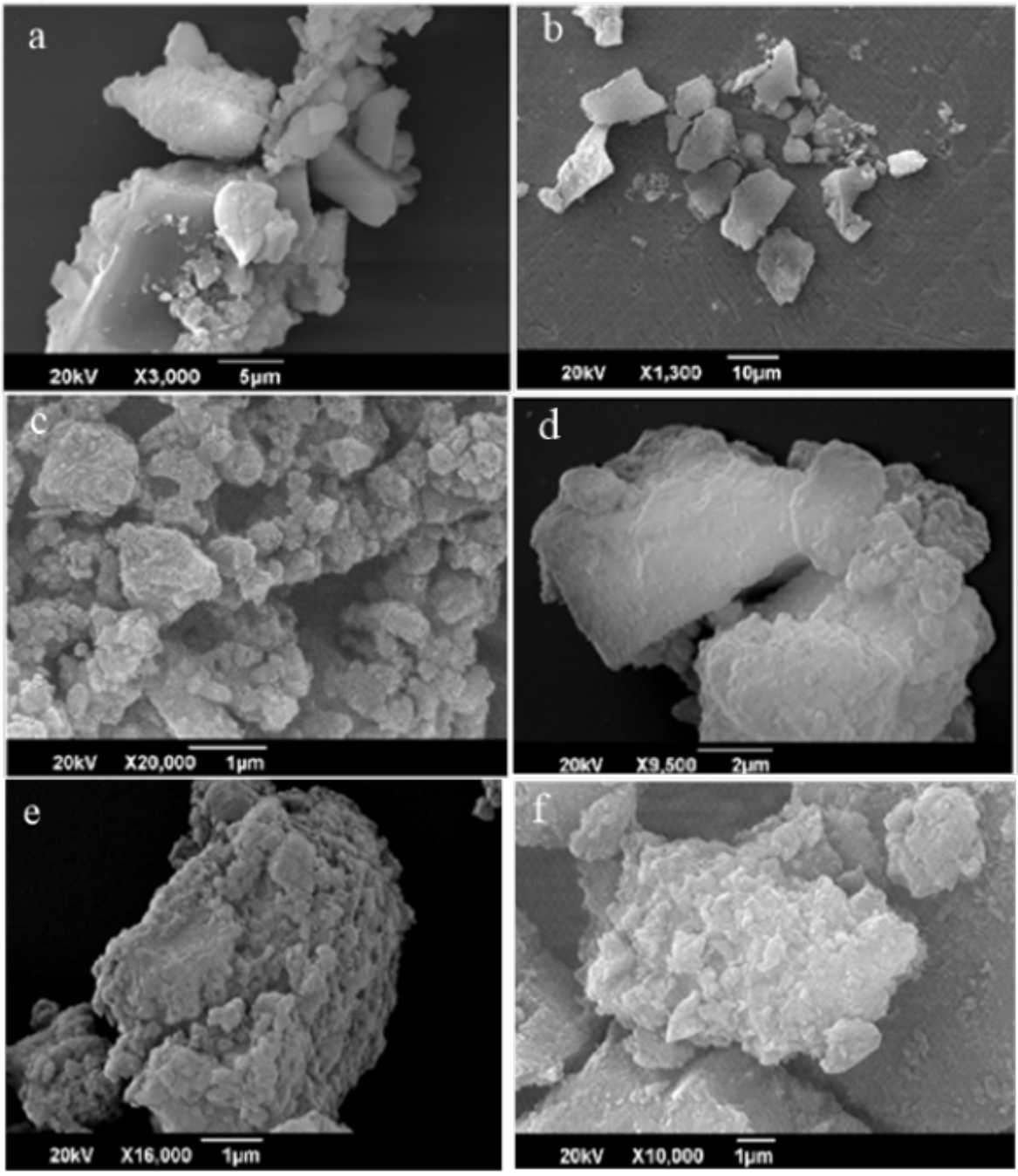

Figure 2. SEM image of batch-1 after 16, 32 and 64 hrs

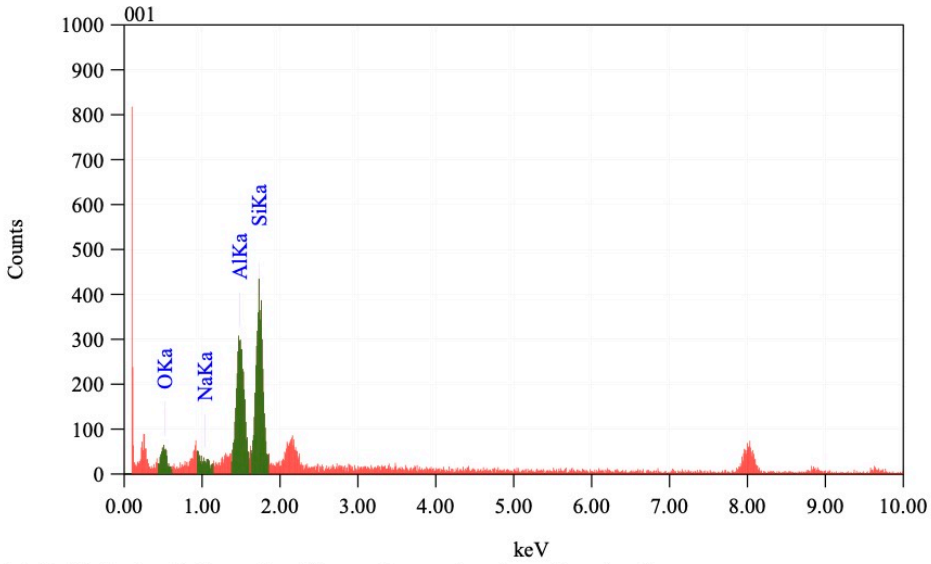

ZAF Method Standardless Quantitative Analysis
Fitting Coefficient : 0.7429

Element	(keV)	Mass%	Error%	Atom%	Compound	Mass%	Cation	K
O K	0.525	22.12	3.24	32.93				20.3425
Na K	1.041	1.01	1.49	1.05				1.3122
Al K	1.486	24.84	1.23	21.92				29.3439
Si K	1.739	52.02	1.76	44.10				49.0015
Total		100.00		100.00				

Figure 3. EDX Spectrum of Batch-1

ification of angles and side that is alpha angle is 94.33^0, beta angle is 116.57^0, and gamma angle is 87.65^0. The sides of the crystal lattice unit cell a, b and c are $8.138A^0$, $12.7890A^0$ and $7.1560A^0$respectively[37–38]. The XRD and reference pattern expressions in figure-8 (a) for batch-1 collecting after 16h, 32h and 64h. The pattern expressions different peaks which match to the XRD pattern of Sodium TectoAluminotrisilicate (PDF reference no. 01-089-6427). The XRD pattern are shown in figure-8 (b). Here also pattern shows Sodium TectoAluminotrisilicate (PDF reference no. 01-071-1151). The XRD pattern for batch-3 are shown in figure-8 (c). Here also pattern indicates Sodium TectoAluminotrisilicate (PDF reference no. 01-071-6218)

Brunauer-Emmett-Teller (BET Analysis of Zeolite)

The analysis parameter was equilibrium base, timed was 5s, saturated pressure was about 760mm of Hg, free space differences ranges from -2.9737cm^3 to -0.0947cm^3, sample density was 1.000 g/cm^3, evacuated rate was 1000 mm of Hg. As surface area is inversely proportional to pore size, increases in size surface area decreases, small pore size has large surface area and vice versa. The surface area, pore size and pore volume of the Zeolite (Sodium TectoAluminotrisilicate) samples obtained after processing for 16h, 32h and 64h are measured by BET technique. The relevant data summarized in Table 2(a) and (b). As shown in table (a), the surface area of the sodium TectoAluminotrisilicate decreases as the processing time increases. The surface area of zeolite sample taken after 16h is 344.9944 m^2/g while surface area for the sample taken after 32h and 64h are 338.7048 m^2/g and 266.9330 m^2/g respectively. This indicates that as the processing time increases the particle size increases thus surface area decreases.

shows with the addition of additive as CNTs the surface area increases, as the time goes on increases from 16h to 64h while the surface area of GO decreases as the time goes on increases from 16h to 64h. After 16h surface area was 292.3505 m^2/g while the surface area after 32h and 64h were 298.1724 m^2/g and 314.3314 m^2/g respectively. These data reveal that as the processing time increases pore size decreases thus surface area increases. The surface area after16h is 234.6936 m^2/g which means

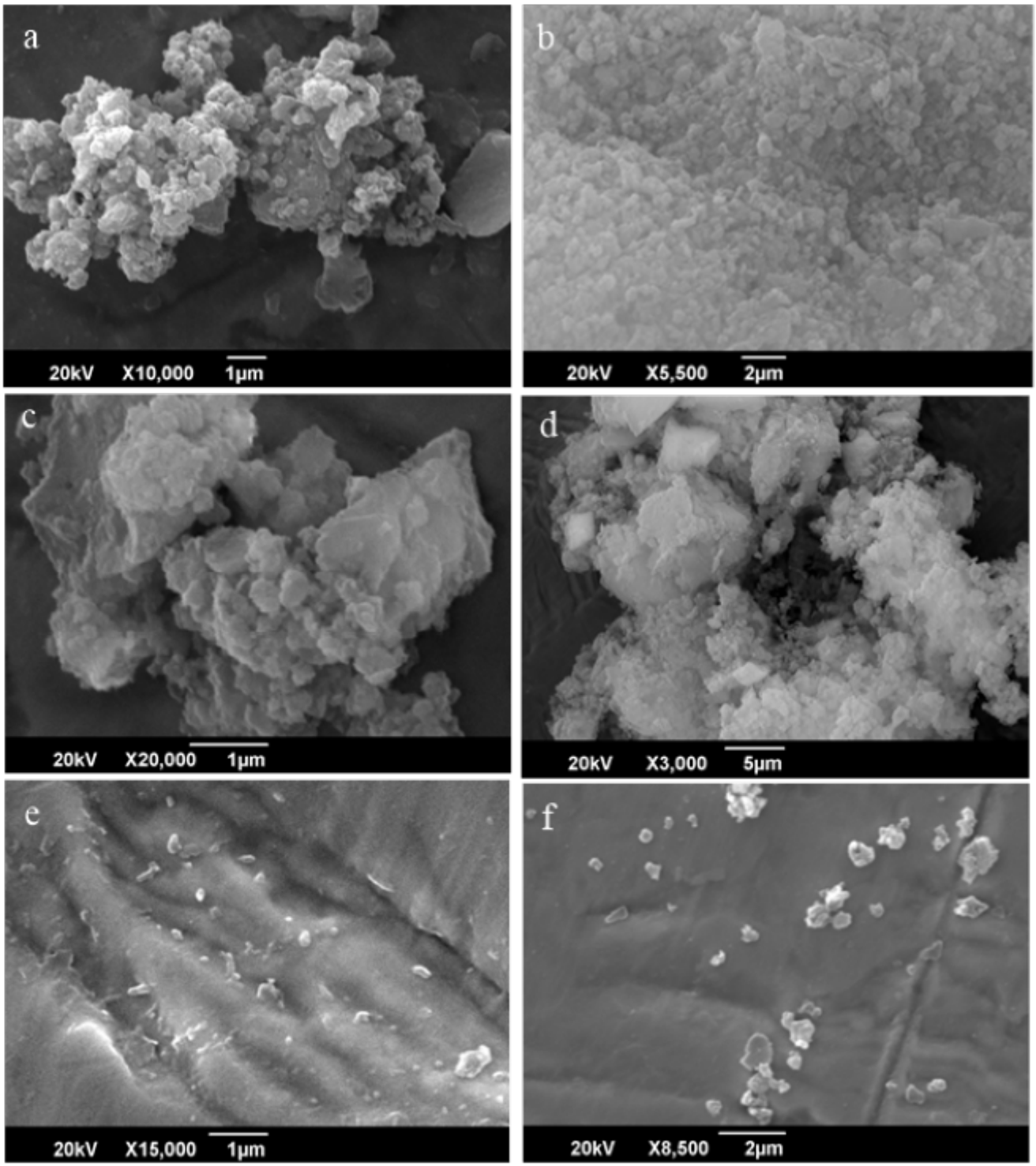

Figure 4. SEM image of batch-2 after 16, 32 and 64 hrs

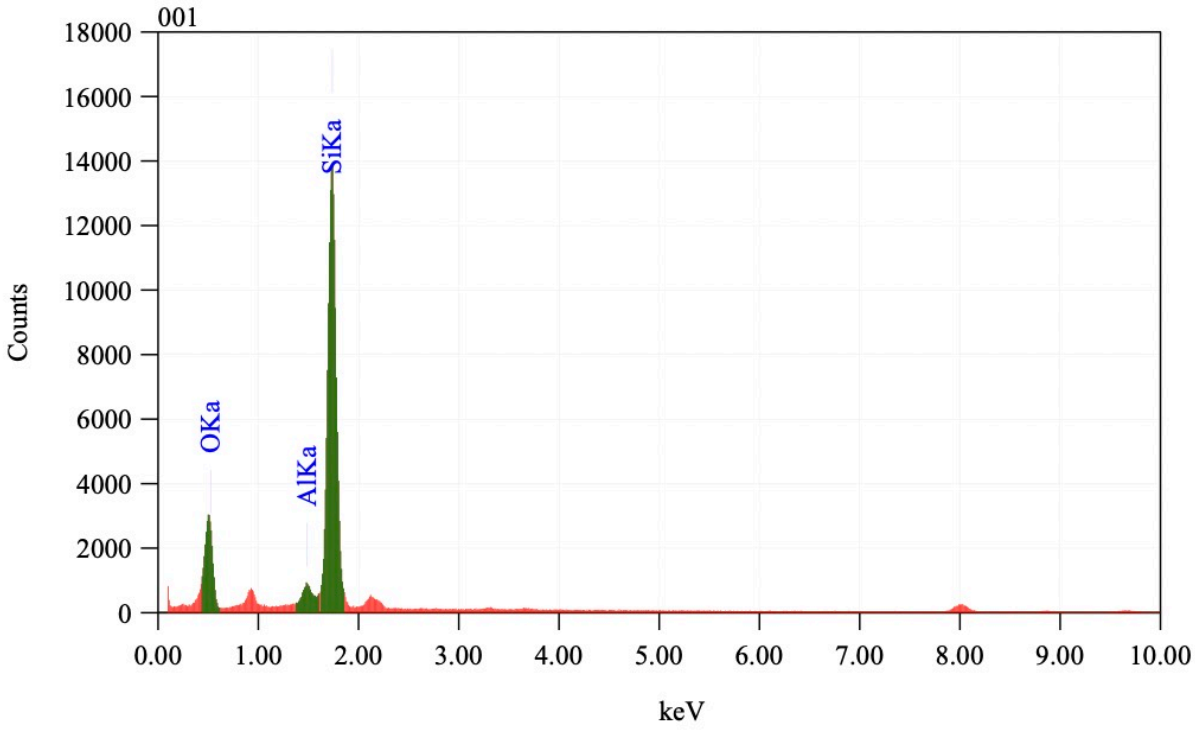

ZAF Method Standardless Quantitative Analysis
Fitting Coefficient : 0.4880

Element	(keV)	Mass%	Error%	Atom%	Compound	Mass%	Cation	K
O K	0.525	38.82	1.17	52.64				35.5718
Al K	1.486	3.13	0.54	2.51				3.0385
Si K	1.739	58.05	0.56	44.84				61.3897
Total		100.00		100.00				

Figure 5. EDX Analysis of Batch-2.

Table 2. ***(a).*** *Surface Area of Zeolite with and without Additive*

Samples	BET surface area of zeolite (m^2/g)	BET surface area of CNTs as additive (m^2/g)	BET surface area of GO as additives (m^2/g)
After 16hour	344.9944	292.3505	234.6936
After 32hour	338.7048	298.1724	127.7253
After 64hour	266.9330	314.3317	107.7345

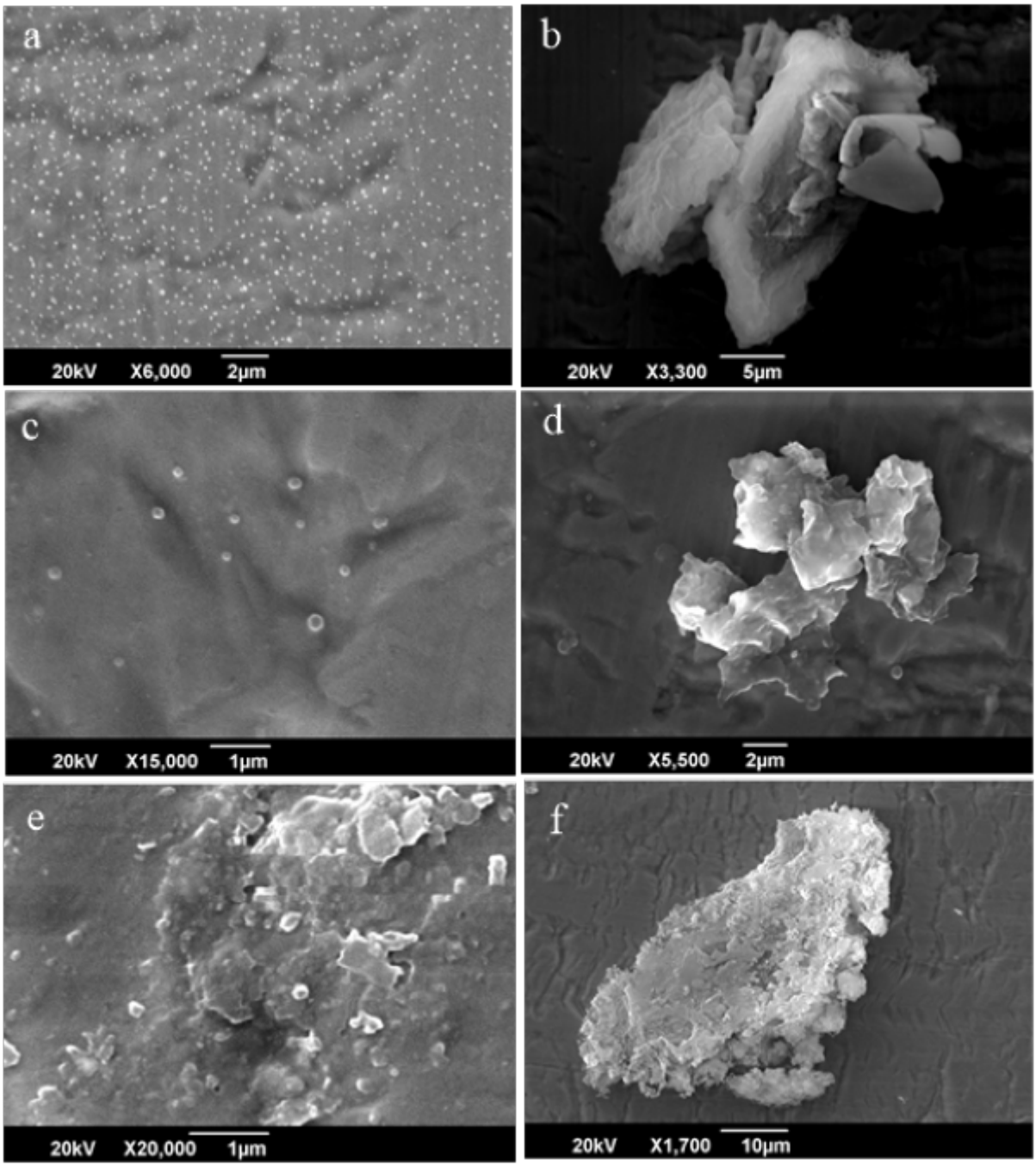

Figure 6. SEM Image of the Batch-3 after 16, 32 and 64 hrs.

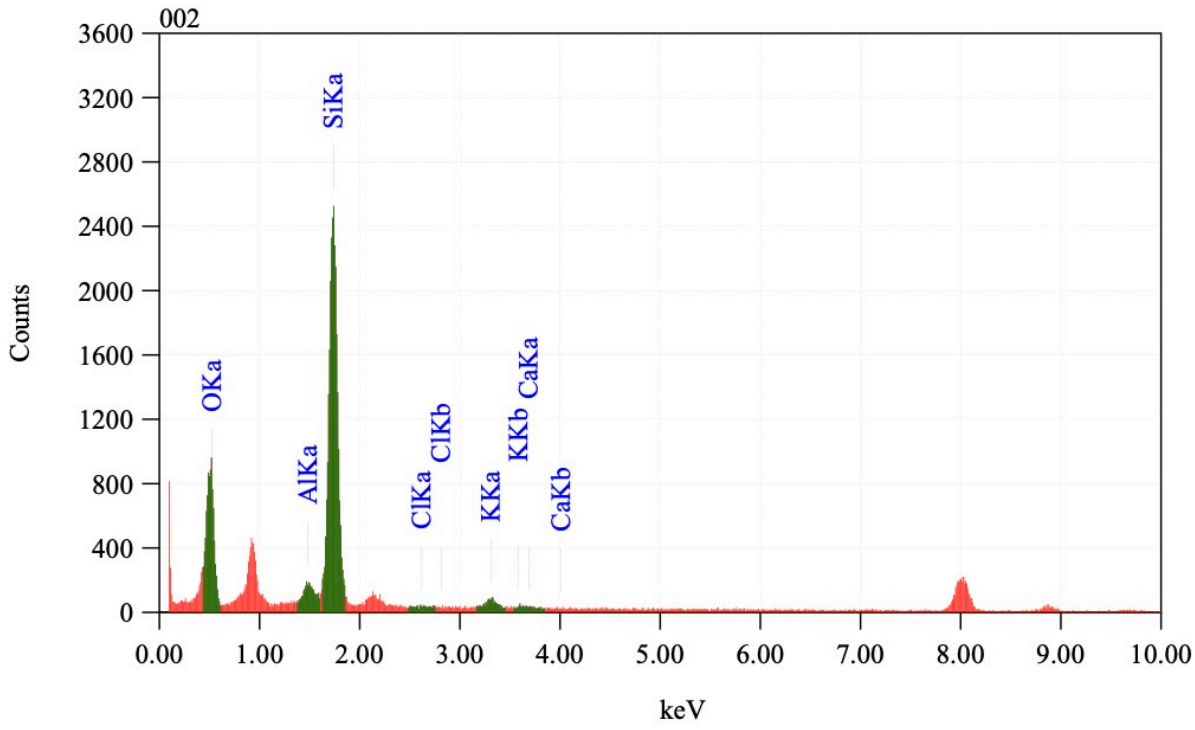

Element	(keV)	Mass%	Error%	Atom%	Compound	Mass%	Cation	K
O K	0.525	49.20	0.97	63.18				48.7332
Al K	1.486	2.63	0.52	2.00				2.3716
Si K	1.739	46.17	0.53	33.77				46.7118
Cl K	2.621	0.06	0.64	0.03				0.0549
K K	3.312	1.77	0.77	0.93				1.9210
Ca K	3.690	0.18	0.87	0.09				0.2075
Total		100.00		100.00				

Figure 7. EDX Analysis of Batch-3.

its surface area is small. After 32h and 64h surface area become 187.6208 m^2/g and 176.9163 m^2/g respectively. These results show that as processing time increases surface area decreases, its pore size increases.

(b) shows that, pore volume of sodium TectoAluminotrisilicate crystal ranges between 18.3A^0 to 18.4A^0. This show that as pore size increases its surface area and catalytic efficiency decreases. As the sample taken after 16h, 32h and 64h pore sizes increases gradually. The average pore size width is also increases as we move from 16h to 64h. The pore size of Zeolite-GO composite samples after 16h, 32h and 64h respectively. The data revealed that pore size with respect to surface area decreases as surface area increases. As table 2 (c) gives the comparative data of surface area and pore size of batch-1, 2 and 3.

Analysis of Zeolite Coated Kevlar Membrane

Figure 9 (a) directs the Kevlar fabric with polymer coated membrane, the PP layer interact with the fiber of Kevlar and form a cage. In figure 9 (b) by the addition of catalyst in coated membrane, its cage like structure trapped the particles and become a composite membrane. Images shows that the interaction between the layer and catalytic layer are properly compatible with fabric.

Tensile strength

For the proving of strength between Kevlar fabrics, Kevlar supported polypropylene membrane and catalyst containing polymer fabric mechanical test applied. For that parameter adjusted and it is clear from data, cata-

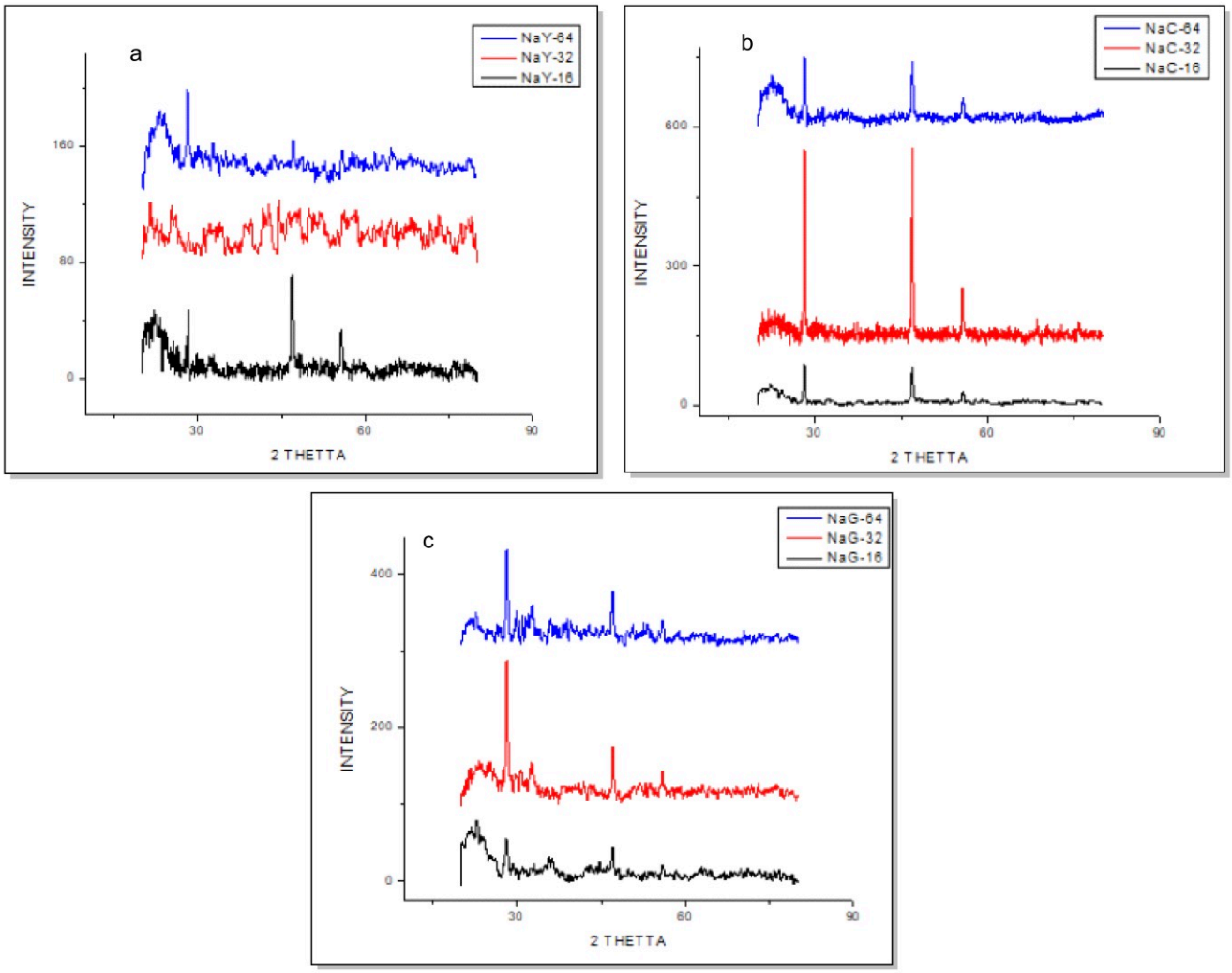

Figure 8. XRD Pattern of batch-1, batch-2 and batch-3

Table 3. ***(b).*** *Pore Volume of Zeolite with and without Additive*

Samples	**Adsorption average pore width without additives (4V/A by BET)**	**Adsorption average pore width of CNTs (4V/A by BET)**	**Adsorption average pore width of GO (4V/A by BET)**
After 16hour	$18.2111A^0$	$18.2864A^0$	$17.9567A^0$
After 32hour	$18.2461A^0$	$18.2640A^0$	$18.2988A^0$
After 64hour	$18.4695A^0$	$18.2524A^0$	$18.4009A^0$

Table 4. Comparative study of Batch-1, 2 & 3

Batches	Sample collection time	BET surface area (m^2 /g)	Pore volume (cm^3 /g)	Pore diameter (A^0)
	16	344.9944	0.217686	18.2111A^0
Batch-1	32	338.7048	0.208979	18.2461A^0
	64	266.9330	0.078368	18.4695A^0
	16	292.3505	0.182356	18.2864A^0
Batch-2	32	298.1724	0.182753	18.2640A^0
	64	314.3317	0.194109	18.2524A^0
	16	234.6936	0.093822	17.9567A^0
Batch-3	32	127.7253	0.080230	18.2988A^0
	64	107.7345	0.080340	18.4009A^0

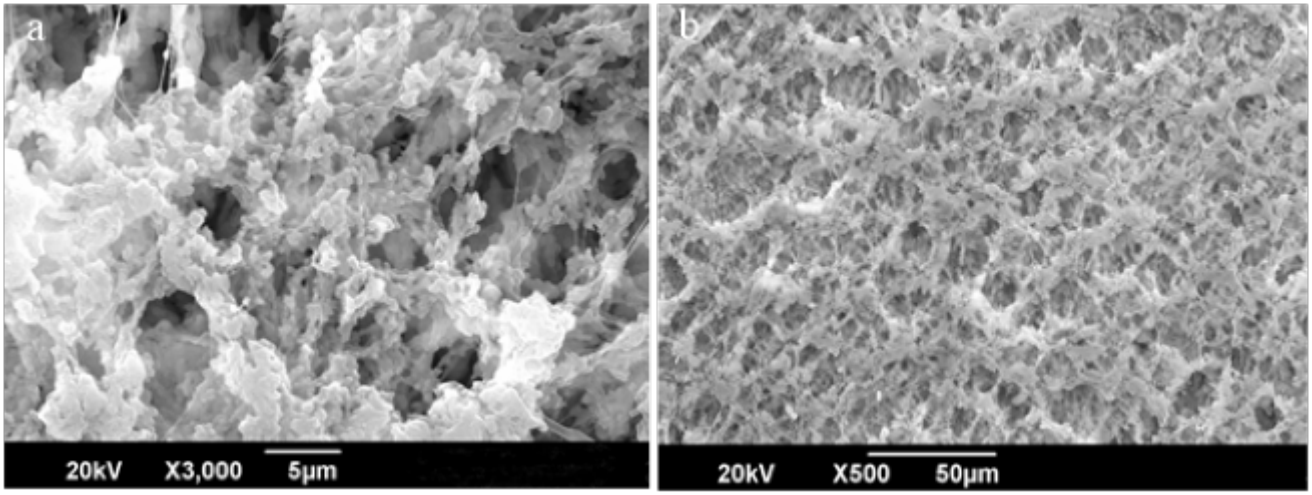

Figure 9. Kevlar Fabric with Polymer Membrane and Catalytic Membrane.

Table 5. Comparison between Kevlar Fiber, PP Membrane and with Composite Membrane of Kevlar

Samples	Kevlar fabric	Kevlar supported polymer membrane	Kevlar supported composite polymer membrane
Parameter unit	1*1	1*1	1*1
Break force sensitivity(N)	10	10	10
Break stress sensitivity(N/mm)	10	10	10
Break strain sensitivity (%)	10	10	10
Max. force calc. at entire area (N)	246.035	151.695	151.695
Max. stress calc. at entire area (N/mm2)	70.2958	43.3413	43.3413
Max. Strain calc. at entire area (%)	2.87303	2.16530	2.16530
Min. force calc. at entire area (N)	-0.0223	0.11126	0.11126
Min. stress calc. at entire area (N/mm2)	-0.0064	0.03179	0.03179
Min. strain calc. at entire area (%)	0.01008	0.01511	0.01511

lyst does not affect mechanical strength of polymeric fabric Kevlar. As the fabrics damages with the increase in temperature, by the addition of zeolite fabric temperature can be manages. Albite does not damage the strength of fabric. It also gives stability with temperature.

CONCLUSIONS

It is settled from the analysis that, additives play a vital role in the morphology of zeolite. We used reflux condensation process assisted by organic templates. Analysis revealed the formation of Albite (Sodium TectoAluminotrisilicate). For analysis we used the techniques FTIR, BET, SEM, EDX and XRD. These helped us to determine morphology, surface area, pore volume, pore size and crystalline geometry. To check variation in Albite, we do not change the Si/Al ratio, only addition of additives which can bring changes. With additives, it can change the pore size, pore volume surface area, crystallinity, composition of Zeolite as well. As time increases, it does not belong to Nano crystal because as aging time increases, size of the crystal goes on increases, it becomes a large molecule rather than a small Nano crystal. SEM analysis revealed, size of particles ranges from 20nm to 100nm for which magnification of the instrument ranges to 50,000 to 1500. It shows regular morphology and size of the particles. Above we presented results which shows the regularity of the geometry and the size of the particle. FTIR outcomes indicated, the composition of Albite that ranges between 1100 cm^{-1} to 900 cm^{-1}. With the addition of additive, it is also clear that formation of Zeolite series between 1100 cm^{-1} to 900 cm^{-1}.BET results shows that with the change in the time, it moves 16h to 32h and then to 64h, its morphology changes as aging time increases its size would become large. With the addition of additives its physical characteristic changes as pore sizes increases or decreases and pore volume also changes to some extent and importantly pore size that depends upon pore volume as well. Surface area of the sample is also an important feature of this characterization. XRD results shows the formation of structure, over here Zeolite formed with a common name as sodium tecto-alumotrisilicate ($AlNaO_8Si_3$). For the practical point of view, Kevlar supported polymer membrane with the Zeolite as catalyst is used. Kevlar fabric is an important fabric used in many ways as in industrial cables, asbestos replacement brake limning, under water treatment application bicycle and racing cars tyres, and importantly body armor as an application. Results show that polymeric supported fabric and catalyst supported fabric have same result with response to mechanical testing.

ACKNOWLEDGMENTS

This work was sponsored by Higher Education Commission; Pakistan (Ref. No. 527/IPFP-II (Batch-I)/SRGP/NAHE/HEC/2020/275).

Data availability Statement

All data analyzed during this study are included in this published article.

References

1) Devos, J.; Borms, R.; Robijns, S.; Ivanushkin, G.; Khalil, I.; Dusselier, M. Engineering low-temperature ozone activation of zeolites: Process specifics, possible mechanisms and hybrid activation methods. *Chemical Engineering Journal* **2022**, *431*, 133862–133862, DOI: 10.1016/j.cej.2021.133862, available at https://dx.doi.org/10.1016/j.cej.2021.133862.
2) Sokol, H. J.; Ebrahim, A. M.; Caratzoulas, S.; Frenkel, A. I.; Valla, J. A. Situ XAFS, XRD, and DFT Characterization of the Sulfur Adsorption Sites on Cu and Ce Exchanged Y Zeolites. *The Journal of Physical Chemistry C* **2022**, *126* (3), 1496–1512.
3) Yang, J.; He, Y.; He, J.; Liu, Y.; Geng, H.; Chen, S.; Lin, L.; Liu, M.; Chen, T.; Jiang, Q.; Weckhuysen, B. M.; Luo, W.; Wu, Z. Enhanced Catalytic Performance through In Situ Encapsulation of Ultrafine Ru Clusters within a High-Aluminum Zeolite. *ACS Catalysis* **2022**, *12* (3), 1847–1856, DOI: 10.1021/acscatal.1c05012, available at https://dx.doi.org/10.1021/acscatal.1c05012.
4) Rimaz, S.; Kosari, M.; Zarinejad, M.; Ramakrishna, S. A comprehensive review on sustainability-motivated applications of SAPO-34 molecular sieve. *Journal of Materials Science* **2022**, *57* (2), 848–886, DOI: 10.1007/s10853-021-06643-1, available at https://dx.doi.org/10.1007/s10853-021-06643-1.
5) Yu, F.; Xiao, F. S. In *eds. Functional Materials from Colloidal Self-assembly.*; and others„ Ed.; John Wiley & Sons, 2022; Vol. 2022; pp 397–453.
6) Shamzhy, M.; Opanasenko, M.; Concepción, P.; Martínez, A. New trends in tailoring active sites in zeolite-based catalysts. *Chemical Society Reviews* **2019**, *48* (4), 1095–1149, DOI: 10.1039/c8cs00887f, available at https://dx.doi.org/10.1039/c8cs00887f.
7) Dehghan, R.; Anbia, M. Zeolites for adsorptive desulfurization from fuels: A review. *Fuel Processing Technology* **2017**, *167*, 99–116, DOI: 10.1016/j.fuproc.2017.06.015, available at https://dx.doi.org/10.1016/j.fuproc.2017.06.015.
8) Möller, K.; Bein, T. Mesoporosity – a new dimension for zeolites. *Chemical Society Reviews* **2013**, *42* (9), 3689–3689, DOI: 10.1039/c3cs35488a, available at https://dx.doi.org/10.1039/c3cs35488a.
9) Jia, X.; Khan, W.; Wu, Z.; Choi, J.; Yip, A. C. Modern synthesis strategies for hierarchical zeolites: Bottom-up versus top-down strategies. *Advanced Powder Technology* **2019**, *30* (3), 467–484, DOI: 10.1016/j.apt.2018.12.014, available at https://dx.doi.org/10.1016/j.apt.2018.12.014.
10) Rassouli, L.; Naderi, R.; Mahdavain, M. Study of the impact of sequence of corrosion inhibitor doping in zeolite on the self-healing properties of silane sol–gel film. *Journal of Industrial and Engineering Chemistry* **2018**, *66*, 221–230, DOI: 10.1016/j.jiec.2018.05.033, available at https://dx.doi.org/10.1016/j.jiec.2018.05.033.
11) Calabrese, L.; Proverbio, E. A Brief Overview on the Anticorrosion Performances of Sol-Gel Zeolite Coatings. *Coatings* **2019**, *9* (6), 409–409, DOI: 10.3390/coatings9060409, available at https://dx.doi.org/10.3390/coatings9060409.
12) Thompson, R. W. Recent Advances in the Understanding of Zeolite Synthesis. *Synthesis* **1998**, 1–33.
13) Rehman, W. U.; Wang, H.; Manj, R. Z. A.; Luo, W.; Yang, J. When Silicon Materials Meet Natural Sources: Opportunities and Challenges for Low-Cost Lithium Storage. *Small* **2021**, *17* (9), 1904508–1904508.
14) Kerstens, D.; Smeyers, B.; Waeyenberg, J. V.; Zhang, Q.; Yu, J.; Sels, B. F. State of the Art and Perspectives of Hierarchical Zeolites: Practical Overview of Synthesis Methods and Use in Catalysis. *Advanced Mate-*

rials **2020**, *32* (44), 2004690–2004690, DOI: 10.1002/adma.202004690, available at https://dx.doi.org/10.1002/adma.202004690.
15) Ríos, C. A.; Williams, C. D.; Roberts, C. L. Removal of heavy metals from acid mine drainage (AMD) using coal fly ash, natural clinker and synthetic zeolites. *Journal of Hazardous Materials* **2008**, *156* (1-3), 23–35, DOI: 10.1016/j.jhazmat.2007.11.123, available at https://dx.doi.org/10.1016/j.jhazmat.2007.11.123.
16) Weitkamp, J. Zeolites and catalysis. *Solid State Ionics* **2000**, *131* (1-2), 175–188, DOI: 10.1016/s0167-2738(00)00632-9, available at https://dx.doi.org/10.1016/s0167-2738(00)00632-9.
17) Mumpton, F. A. La roca magica: Uses of natural zeolites in agriculture and industry. *Proceedings of the National Academy of Sciences* **1999**, *96* (7), 3463–3470, DOI: 10.1073/pnas.96.7.3463, available at https://dx.doi.org/10.1073/pnas.96.7.3463.
18) Dusselier, M.; Davis, M. E. Small-Pore Zeolites: Synthesis and Catalysis. *Chemical Reviews* **2018**, *118* (11), 5265–5329, DOI: 10.1021/acs.chemrev.7b00738, available at https://dx.doi.org/10.1021/acs.chemrev.7b00738.
19) McMorn, P.; Hutchings, G. J. Heterogeneous enantioselective catalysts: strategies for the immobilisation of homogeneous catalysts. *Chemical Society Reviews* **2004**, *33* (2), 108–108, DOI: 10.1039/b200387m, available at https://dx.doi.org/10.1039/b200387m.
20) Grand, J.; Awala, H.; Mintova, S. Mechanism of zeolites crystal growth: new findings and open questions. *CrystEngComm* **2016**, *18* (5), 650–664, DOI: 10.1039/c5ce02286j, available at https://dx.doi.org/10.1039/c5ce02286j.
21) Liu, Z.; Okabe, K.; Anand, C.; Yonezawa, Y.; Zhu, J.; Yamada, H.; Endo, A.; Yanaba, Y.; Yoshikawa, T.; Ohara, K.; Okubo, T.; Wakihara, T. Continuous flow synthesis of ZSM-5 zeolite on the order of seconds. *Proceedings of the National Academy of Sciences* **2016**, *113* (50), 14267–14271, DOI: 10.1073/pnas.1615872113, available at https://dx.doi.org/10.1073/pnas.1615872113.
22) Chen, N. Y.; Degnan, T. F.; Smith, C. M. In *Molecular transport and reaction in zeolites: design and application of shape selective catalysis*; and others„ Ed.; John Wiley & Sons, 1994.
23) Rhodes, C. J. Zeolites: physical aspects and environmental applications. *Annual Reports Section "C" (Physical Chemistry)* **2007**, *103*, 287–287.
24) Füllbrandt, M.; Purohit, P. J.; Schönhals, A. Combined FTIR and dielectric investigation of poly (vinyl acetate) adsorbed on silica particles. *Macromolecules* **2013**, *46* (11), 4626–4632.
25) Aroke, U.; El-Nafaty, U.; Xrf, XRD and FTIR properties and characterization of HDTMA-Br surface modified organo-kaolinite clay. *International Journal of Emerging Technology and Advanced Engineering 2014* (4), 817–825.
26) Mozgawa, W. The influence of some heavy metals cations on the FTIR spectra of zeolites. *Journal of Molecular Structure* **2000**, *555* (1-3), 299–304, DOI: 10.1016/s0022-2860(00)00613-x, available at https://dx.doi.org/10.1016/s0022-2860(00)00613-x.
27) Palomino, G. T.; Carayol, M. R. L.; Areán, C. O. Hydrogen adsorption on magnesium-exchanged zeolites. *J. Mater. Chem.* **2006**, *16* (28), 2884–2885, DOI: 10.1039/b607261e, available at https://dx.doi.org/10.1039/b607261e.
28) Pyra, K.; Tarach, K. A.; Janiszewska, E.; Majda, D.; Góra-Marek, K. Evaluation of the Textural Parameters of Zeolite Beta in LDPE Catalytic Degradation: Thermogravimetric Analysis Coupled with FTIR Operando Studies. *Molecules* **2020**, *25* (4), 926–926, DOI: 10.3390/molecules25040926, available at https://dx.doi.org/10.3390/molecules25040926.
29) Sadrara, M.; Khorrami, M. K.; Darian, J. T.; Garmarudi, A. B.; Yaripour, F.; Noor, P. Investigation of mesopore volume of ZSM-Type zeolites by diffuse reflectance FTIR spectroscopy and multivariate calibration. *Infrared Physics & Technology* **2020**, *105*, 103222–103222, DOI: 10.1016/j.infrared.2020.103222, available at https://dx.doi.org/10.1016/j.infrared.2020.103222.
30) Ahmed, S.; Cai, Y.; Ali, M.; Khanal, S.; Xu, S. Preparation and performance of nanoparticle-reinforced chitosan proton-exchange membranes for fuel-cell applications. *Journal of Applied Polymer Science* **2019**, *136* (1), 46904–46904, DOI: 10.1002/app.46904, available at https://dx.doi.org/10.1002/app.46904.
31) Ahmed, S.; Cai, Y.; Ali, M.; Khannal, S.; Xu, S. Preparation and properties of alkyl benzene sulfonic acid coated boehmite/chitosan nanocomposite membranes with enhanced proton conductivity for proton exchange membrane fuel cells. *Materials Express* **2019**, *9* (1), 42–50, DOI: 10.1166/mex.2019.1468, available at https://dx.doi.org/10.1166/mex.2019.1468.
32) Ahmed, S.; Cai, Y.; Ali, M.; Khannal, S.; Ahmad, Z.; Lu, Y.; Wang, S.; Xu, S. One-step phosphorylation of graphene oxide for the fabrication of nanocomposite membranes with enhanced proton conductivity for fuel cell applications. *Journal of Materials Science: Materials in Electronics* **2019**, *30* (14), 13056–13066, DOI: 10.1007/s10854-019-01667-5, available at https://dx.doi.org/10.1007/s10854-019-01667-5.
33) Ahmed, S.; Ali, M.; Cai, Y.; Lu, Y.; Ahmad, Z.; Khannal, S.; Xu, S. Novel sulfonated multi-walled carbon nanotubes filled chitosan composite membrane for fuel-cell applications. *Journal of Applied Polymer Science* **2019**, *136* (22), 47603–47603, DOI: 10.1002/app.47603, available at https://dx.doi.org/10.1002/app.47603.
34) Hassan, M.; Afzal, A.; Tariq, M.; Ahmed, S. Synthesis of the hyper-branched polyamides and their effective utilization in adsorption and equilibrium isothermal study for cadmium ion uptake. *Journal of Polymer Research* **2021**, *28* (6), 1–11, DOI: 10.1007/s10965-021-02554-6, available at https://dx.doi.org/10.1007/s10965-021-02554-6.
35) Luukkonen, T.; Abdollahnejad, Z.; Yliniemi, J.; Kinnunen, P.; Illikainen, M. One-part alkali-activated materials: A review. *Cement and Concrete Research* **2018**, *103*, 21–34, DOI: 10.1016/j.cemconres.2017.10.001, available at https://dx.doi.org/10.1016/j.cemconres.2017.10.001.
36) Pathak, A. A laboratory scale synthesis of geopolymer from construction wastes. 2016.